

Multipoint Simultaneous Tracking of Wireless Capsule Endoscope Using Magnetic Sensor Array

Min Wang^{ID}, Shuang Song^{ID}, Jun Liu^{ID}, Member, IEEE, and Max Q.-H. Meng^{ID}, Fellow, IEEE

Abstract—Magnetic tracking has been well studied for the localization of wireless capsule robots. However, most of the existing magnetic localization systems require a stable background magnetic field, which is not suitable for wearable applications as the movement of the human body inevitably changes the magnetic field to each sensor. The purpose of this study is to reduce the disturbance of the ambient magnetic field for localizations in different background scenarios. The proposed approach applies the magnetic density of multiple sampling points for simultaneous localization. By subtracting the magnetic field value in different positions, the background noise (BGN) field can be offset. As a result, multipoint simultaneous positioning can be achieved by using an optimization algorithm. The influence of the signal-to-noise ratio on localization accuracy has been determined through simulation analysis. Experiments first verified the feasibility of multipoint simultaneous positioning and then conducted in different geomagnetic noise and permanent magnet environments. The results show that the proposed method has been verified to be robust in different BGN environments. The proposed method is expected to be used in wearable systems for tracking magnetic capsule endoscope (MCE).

Index Terms—Capsule endoscope, magnetic tracking, multipoint localization.

I. INTRODUCTION

WIRELESS capsule endoscope is preferable to tethered examination tools in the diagnosis of gastrointestinal tract diseases and potentially for interventions because of the unique advantages in low invasiveness and long working time. Using the capsule endoscope as a versatile platform, a variety of applications have been achieved in the past decade, including drug delivery [1], biopsy [2], medical image capture [3], and site-specific thrombolysis [4]. To provide the position of the endoscope inside the human body, a series of tracking approaches are reported, including traditional radio

Manuscript received December 31, 2020; revised April 3, 2021; accepted April 16, 2021. Date of publication April 26, 2021; date of current version May 19, 2021. This work was supported in part by the National Natural Science Foundation of China under Grant 61803123, in part by the Guangdong Basic and Applied Basic Research Fund under Grant 2019A1515110175, and in part by the Research Grants Council (RGC) of Hong Kong under Grant 21212720. The Associate Editor coordinating the review process was Bruno Ando. (*Corresponding authors:* Shuang Song; Jun Liu.)

Min Wang is with the Department of Mechanical Engineering, City University of Hong Kong, Hong Kong, SAR, China.

Shuang Song is with the School of Mechanical Engineering and Automation, Harbin Institute of Technology (Shenzhen), Shenzhen 518055, China (e-mail: songshuang@hit.edu.cn).

Jun Liu is with the Department of Mechanical Engineering, City University of Hong Kong, Hong Kong, SAR, China, and also with the Shenzhen Research Institute, City University of Hong Kong, Shenzhen 518057, China (e-mail: jun.liu@cityu.edu.hk).

Max Q.-H. Meng is with the Department of Electronic and Electrical Engineering, Southern University of Science and Technology, Shenzhen 518055, China.

Digital Object Identifier 10.1109/TIM.2021.3075776

frequency (RF) localization [5], microwave imaging localization [6], and gamma-ray-based localization [7]. Compared to other methods, magnetic localization that tracks the permanent magnets attached to the capsule endoscope is commonly used because of its small size, high safety, and free of power and light. Although magnetic tracking can be disturbed by ferromagnetic materials, one can avoid this by removing or replacing ferromagnetic items with other materials (e.g., ceramic, rubber, and plastic).

In recent years, many researchers have been working on the localization of passive permanent magnets for magnetic capsule robots. Schlageter *et al.* [8] first developed a five-degree-of-freedom (DOF) tracking system based on a magnetic sensor array. The proposed method can achieve a detection range of over 200 mm, but no tracking accuracy is provided. Hu *et al.* [9] reported an improved tracking system with 64 magnetic sensors spreading in a cubic workspace. The reported system can get an average position error of 3.7 mm and an orientation error of 1.8° in a workspace of 0.5 m × 0.5 m × 0.5 m. Other magnetic tracking algorithms attempted to improve the robustness of the tracking system through the integration of an external actuation using either permanent magnets or electromagnetic coils [10]–[12]. These tracking systems can achieve the actuation and localization simultaneously, which is beneficial to the closed-loop control of the miniaturized robots for manipulation.

The mainstream of existing magnetic localization systems utilizes a static sensor array as a reference framework for calculating the position and orientation of the magnetic capsule endoscope (MCE) [13], [14]. However, the magnetic sensor array working under a nonuniform background field or rotational sensor array can lead to the deviation of localization results, as the ambient noise varies significantly in different positions and, therefore, introduces additional errors to the true localization result. To address this problem, Dai *et al.* [15] proposed an IMU integrated magnetic tracking system, which is able to get the real-time pose of the system and then accurately remove geomagnetic noise. Wu *et al.* [16] and Shao *et al.* [17] use additional sensors distributed on the chest to quantify the background noise (BGN). The authors assumed that the sensors on the chest are minimally affected by the targets in the intestine and can be used to accurately sense the ambient magnetic field. Kramer and Kandel [18] compared four filtering algorithms to improve the positioning accuracy of small robots. Hu *et al.* [19] proposed a wearable system using three magnets, where two magnets were fixed to establish a base coordinate system, and the position of the third magnet on the capsule endoscope was obtained under this fixed coordinate

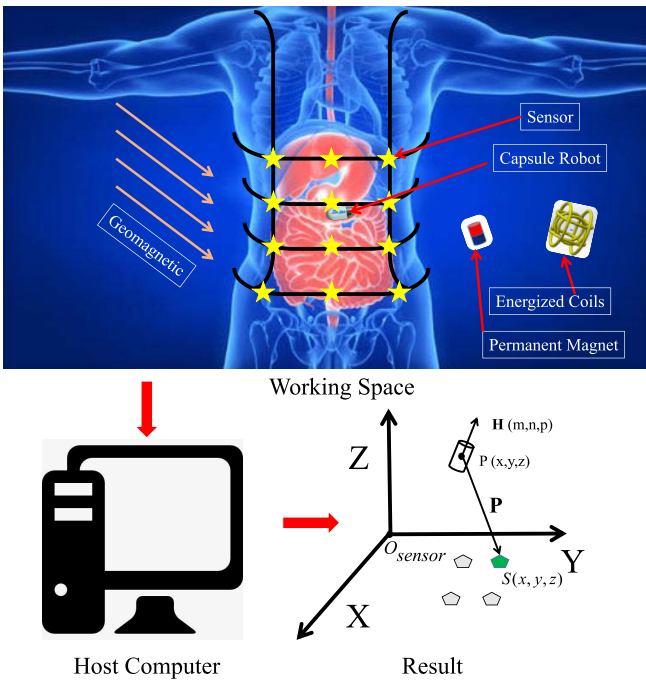


Fig. 1. System overview. Besides the magnetic capsule robot, the geomagnetic field, permanent magnets, or energizing coils also contribute to the entire magnetic field that is monitored by the wearable sensor array. The position and orientation of the capsule robot relative to the sensor array are obtained by the tracking algorithms running on the host computer.

instead of the time-varying coordinate on the wearable sensor array. Compared with the bulky and fixed sensing system, the recent advancement of wearable sensors has generated unprecedented benefits to enable long-time monitoring and examinations with highly improved user experience [20].

Magnetic tracking devices were also used to quantitatively track the movement of the tongue, fingers, and limbs [21]–[24] and indoor localization [25] and achieved a good tracking performance. However, the aforementioned methods rely on a static localization system or are ineffective against the nonuniform interference from the BGN. During the medical examination using a capsule endoscope, the patient often gets up and walks around, causing the position and orientation of the sensor array to change dramatically. When the patient is close to the external magnetic sources (e.g., permanent magnets or electromagnetic coils), the abrupt changes in the BGN can lead to a significant drift in the localization results.

In this work, we address the influence of external noise on localization results. The proposed system is illustrated in Fig. 1. The host computer reads the value of the sensor array from the complex BGN. Through the multipoint simultaneous localization algorithm, the position and orientation of the MCE in the sensor coordinate system can be obtained. To ensure a simple implementation in a wearable system, this new algorithm uses a similar structure as the conventional single point localization [26], [27] and does not require additional hardware.

Compared with conventional methods, the proposed algorithm is able to reduce the BGN through the fusion of multiple measurements and accurate modeling of the magnetic field generated by the localization target. This new algorithm is

robust to the changing environment and has a high potential for practical use to allow patients to move around freely during long-term gastrointestinal track examination.

The rest of this article is organized as follows. The mathematical model and tracking algorithm of the magnetic system is introduced in Section II. A simulation experiment is explained in Section III. The experimental results under different configurations are presented in Section IV. Section V discusses the advantages and limitations of the proposed method. Section VI concludes this work.

II. METHOD

A. Target Magnetic Field

In most magnetic tracking systems, the field sources generated by a cylindrical magnet are captured by an array of magnetoinductive sensors distributed outside the body. In Fig. 1, the magnet is shown as the cylinder at position $P(x, y, z)$, while the magnetoinductive sensors are shown as pentagons at $S(x, y, z)$ in the XY plane. The position and orientation of the magnet target are estimated by analyzing the signals captured by the sensor array. The calculation of the magnetic field is based on the dipole model when the distance between the sensor and the magnet is comparatively larger than the size of the target magnet. In a dipole model, the magnetic intensity generated is defined as

$$\mathbf{B} = B_x \mathbf{i} + B_y \mathbf{j} + B_z \mathbf{k} \\ = \frac{\mu_r \mu_0 M_T}{4\pi} \left(\frac{3(\mathbf{H}_0 \cdot \mathbf{P})\mathbf{P}}{R^5} - \frac{\mathbf{H}_0}{R^3} \right) \quad (1)$$

where $(B_x, B_y, B_z)^T$ is the component of the magnetic intensity parallel to the coordinate axis, μ_r is the relative permeability of air, and μ_0 ($4\pi \times 10^{-7} T \cdot m/A$) is the vacuum permeability. M_T (unit $A \cdot m^2$) is the constant for given material and size of magnet. \mathbf{H}_0 is a normalized vector characterizing the direction of the magnetic moment of the target. \mathbf{P} is the vector pointing from the dipole to the sensor, and R is the module of this vector, where

$$\mathbf{P} = (x - a, y - b, z - c)^T \quad (2)$$

$$R = \sqrt{(x - a)^2 + (y - b)^2 + (z - c)^2}. \quad (3)$$

B. Perceived Magnetic Field Value

In practice, the analog output of the magnetic sensor cannot reflect the actual intensity of the magnetic field due to manufacturing defects. In addition, because of the unevenness of materials and dimensions, M_T is inconstant for the magnet sensors in the array. To approve the measurement accuracy, the calibration progress is indispensable. Here, we use a sensitivity coefficient matrix \mathbf{K} to correct the output of each sensor so that they are closest to the true value.

Define an error function by measured and theoretical values

$$\mathbf{E} = \sum_{i=1}^N \|\mathbf{V}_i - \mathbf{KB}_i\|^2 \quad (4)$$

where $\mathbf{E} = (E_x, E_y, E_z)^T$ is the error value in three axes; N is the number of sampling points; $\mathbf{B}_i = (B_{ix}, B_{iy}, B_{iz})^T$

is the theoretical value of the target; $\mathbf{K} = \begin{bmatrix} k_x & 0 & 0 \\ 0 & k_y & 0 \\ 0 & 0 & k_z \end{bmatrix}$; lowercase k indicates the sensitivity in three axes; and $\mathbf{V}^k_i = (V_{ix}^k, V_{iy}^k, V_{iz}^k)^T$ is the output of the magnetic sensor.

The calibration board is made of an acrylic plate with structural grooves machined by CNC. These predefined locations and orientations of the grooves are considered as the ground truth. During the calibration, the acrylic board is installed at different heights away from the sensor array. An MCE is then placed manually at each groove, and the sensor array records the corresponding output.

Combining the theoretical and measured value in each specific sampling point, the sensitivity coefficient matrix \mathbf{K} can be solved by minimizing the error function in each axis. Taking the x -axis as an example, we have

$$\frac{\partial \sum_{i=1}^N (V_{ix}^k - k_x B_{ix})^2}{\partial k_x} = 0 \quad (5)$$

where i is the number of sampling points, and then, the sensitivity factor in the x -axis can be derived as

$$k_x = \frac{\sum V_{ix}^k \times B_{ix}}{\sum B_{ix} \times B_{ix}}. \quad (6)$$

Before the tracking algorithm is employed, \mathbf{V}^k is divided by \mathbf{K} to approximate the true magnetic field value. In the following discussions, \mathbf{V} represents the output value corrected by the sensitivity coefficient.

In practical applications, the magnetic field measured by the sensors inevitably includes the internal noise from sensors and a variety of BGNs such as geomagnetic noise from the Earth, and interference generated by charged coils or permanent magnets. Therefore, the measured magnetic field value is decomposed as

$$\mathbf{V} = \mathbf{B} + (\mathbf{B}_{\text{bgn}} + \mathbf{B}_{\text{inh}}) \quad (7)$$

where \mathbf{B} is the theoretical magnetic value of MCE; \mathbf{B}_{bgn} is the sum of ambient magnetic field noise from different sources; and \mathbf{B}_{inh} is the inherent noise from the sensor. Since the inherent noise \mathbf{B}_{inh} is due to the fundamental quality and defects of the sensors, it is unavoidable and impossible to remove after the hardware is determined. Therefore, we aim to reduce the impact of BGN \mathbf{B}_{bgn} and improve the system's robustness in a changing environment.

C. Algorithm

Most existing magnetic tracking systems work in a static noise environment. The typical approach to eliminate the influence of noise is to carefully calibrate them before measuring the magnetic field of the real target. The calibrated value is then subtracted from the measured field value. However, the assumption of uniform magnetic noise is not valid in real practice, as the tracking system is often operated in different magnetic environments.

To address this problem, we propose to use the measured values at different positions to minimize the impact of environmental noise. In this new method, the environmental magnetic field and sensor positions are allowed to change during different positioning cycles. Assuming that the MCE moves from

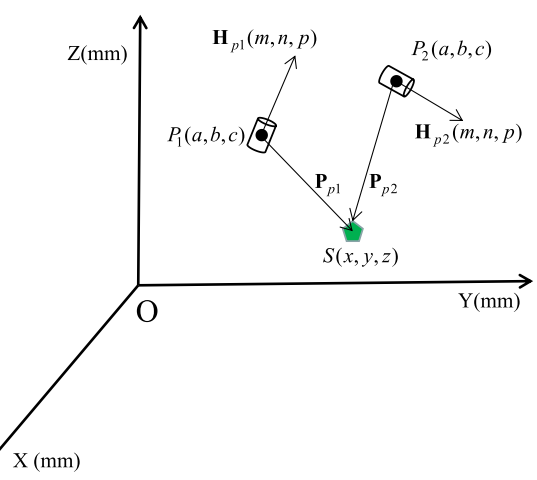


Fig. 2. Position and direction of the same target changes its position from P_1 to P_2 . The distance \mathbf{P} and orientation \mathbf{H} in relative to the sensor $S(x, y, z)$ are obtained by analyzing the magnetic field at the two sampling points.

position P_1 to position P_2 (see Fig. 2), the measured values according to (7) are expressed as

$$\mathbf{B}^{p1} = \mathbf{V}^{p1} - (\mathbf{B}_{\text{bgn}} + \mathbf{B}_{\text{inh}}^{p1}) \quad (8)$$

$$\mathbf{B}^{p2} = \mathbf{V}^{p2} - (\mathbf{B}_{\text{bgn}} + \mathbf{B}_{\text{inh}}^{p2}). \quad (9)$$

Taking the difference between (8) and (9), the environmental noise is removed. Only theoretical values (B), measured values by sensor array (V), and inherent noise (B_{inh}) remain in the following equation:

$$\mathbf{B}^{p2} - \mathbf{B}^{p1} = \mathbf{V}^{p2} - \mathbf{V}^{p1} - (\mathbf{B}_{\text{inh}}^{p2} - \mathbf{B}_{\text{inh}}^{p1}) \quad (10)$$

where $\mathbf{B}_{\text{inh}}^{p2} - \mathbf{B}_{\text{inh}}^{p1} = \mathcal{N}$ indicates the inherent noise. The subscripts $p2$ and $p1$ represent the values at different sample positions.

The position and orientation of the target MCE are optimized by minimizing the error function between the theoretical model and the measured value

$$\mathbf{E}^p = \sum_{i=1}^n \|\Delta \mathbf{B}_i^p - \Delta \mathbf{V}_i^p\|^2 \quad (11)$$

where $\Delta \mathbf{B}_i^p = \mathbf{B}_i^{p2} - \mathbf{B}_i^{p1}$ and $\Delta \mathbf{V}_i^p = \mathbf{V}_i^{p2} - \mathbf{V}_i^{p1}$ are the difference between the theoretical and measured magnetic strengths acting on the i th sensor from the MCE at positions $p1$ and $p2$, respectively; n indicates the number of sensors in the sensor array. By minimizing the error function in (11), the multipoint simultaneous positioning algorithm is converted to the optimization of the objective function

$$(P_1, \mathbf{H}_{p1}, P_2, \mathbf{H}_{p2}) = \arg \min \sum_{i=1}^n \|\Delta \mathbf{B}_i^p - \Delta \mathbf{V}_i^p\|^2 \quad (12)$$

$$\text{s.t. } m_{p1}^2 + n_{p1}^2 + p_{p1}^2 = 1 \quad (13)$$

$$m_{p2}^2 + n_{p2}^2 + p_{p2}^2 = 1 \quad (14)$$

where (a_{p1}, b_{p1}, c_{p1}) and (a_{p2}, b_{p2}, c_{p2}) represent the target position in position $p1$ and position $p2$ in the Cartesian coordinate system; (m_{p1}, n_{p1}, p_{p1}) and (m_{p2}, n_{p2}, p_{p2}) are the unit orientation vectors of the target at positions $p1$ and $p2$, respectively.

The localization result of the conventional method is achieved by minimizing the differences between the measured results and the theoretical values at a one-time point, as follows:

$$(P, \mathbf{H}) = \arg \min \sum_{l=1}^n \|\mathbf{B}_i - \mathbf{V}_i\|^2. \quad (15)$$

According to (7), there exist BGN when directly optimization. As a result, the localization accuracy will shift and unstable.

In (12)–(14), a localization system with N_{sen} triaxis sensors is able to achieve N_{pos} number of simultaneous positioning points. The total number of unknown terms N_{unk} and the number of equations N_{equa} are expressed as follows:

$$\begin{aligned} N_{\text{unk}} &= 6 \times N_{\text{pos}} \\ N_{\text{equa}} &= 3 \times N_{\text{sen}} + N_{\text{pos}}. \end{aligned} \quad (16)$$

To make sure that (11) can be solved, the number of equations should be more than the number of unknown parameters (i.e., $N_{\text{equa}} > N_{\text{unk}}$). Therefore, (15) can be rewritten as

$$3 \times N_{\text{sen}} > 5 \times N_{\text{pos}}. \quad (17)$$

In this article, the localization system consists of eight ($N_{\text{sen}} = 8$) sensors. At most four points can be used simultaneously for positioned. However, the larger N_{pos} will reduce the redundancy of the equations and affect the optimization effect. As a proof, we employ two ($N_{\text{pos}} = 2$) sampling points in the experiments for simultaneous localization. It is able to get the solution according to (16). With the above condition, an initial guess of the position and orientation of the MCE is achieved by the particle swarm optimization (PSO) algorithm. To further improve the performance, a subsequent estimation is completed by the Levenberg–Marquard (LM) algorithm. The proposed method that alleviates the negative effect of BGN on positioning accuracy via fusing multiset of sensor's output is summarized in Algorithm 1.

D. Signal Quality Characterization

The proposed multipoint simultaneous localization is able to reduce the effect of BGN and, therefore, increase the signal-to-noise ratio. However, the proposed algorithm relies on the difference of the magnetic field at different positions, and the sampling distance (S-D) between the simultaneously located points can affect the positioning accuracy. To investigate the optimal working conditions for the proposed method, a new parameter is employed to quantify the quality of the sensed signal.

From the error function (11), the quality of the signal increases with the theoretical difference $\Delta \mathbf{B}^p = \mathbf{B}^{p2} - \mathbf{B}^{p1}$, whereas the internal noise difference $\mathcal{N} = \mathbf{B}_{\text{inh}}^{p2} - \mathbf{B}_{\text{inh}}^{p1}$ has a negative effect on the final results. Therefore, the new quantification parameter is defined as the signal quality ratio (SQR) by calculating the ratio of the theoretical difference over the differences of inherent noise at positions $P1$ and $P2$

$$\text{SQR} = \left| \frac{\|\mathbf{B}^{p2}\| - \|\mathbf{B}^{p1}\|}{\|\mathbf{B}_{\text{inh}}^{p2}\| - \|\mathbf{B}_{\text{inh}}^{p1}\|} \right|. \quad (18)$$

Algorithm 1 Multipoint Simultaneously Magnetic Tracking

Input: Sensor array position: \mathbf{P}_i ; Initial point and orientation: $P_1^{\text{init}}, \mathbf{H}_p^{\text{init}}, P_2^{\text{init}}, \mathbf{H}_p^{\text{init}}$; Calibration matrix: \mathbf{K}
Output: Real-time position and orientation of magnet: $P_1, \mathbf{H}_p, P_2, \mathbf{H}_p$

```

1: repeat
2:   Sensor array output at p1:  $\mathbf{V}_i^{p1}$ 
3:   Theoretical calculation at p1:  $\mathbf{B}_i^{p1}$ 
4:   Sensor array output at p2:  $\mathbf{V}_i^{p2}$ 
5:   Theoretical calculation at p2:  $\mathbf{B}_i^{p2}$ 
6:   Calibration output:  $\mathbf{V}_i^p = \mathbf{V}_i^{p1}/\mathbf{K}$ 
7:   Fusion of sensor measurement:  $\Delta \mathbf{V}_i^p = \mathbf{V}_i^{p2} - \mathbf{V}_i^{p1}$ 
8:   Calculate theoretical difference:  $\Delta \mathbf{B}_i^p = \mathbf{V}_i^{p2} - \mathbf{V}_i^{p1}$ 
9:   Define error function:  $\mathbf{E}^p = \sum_{i=1}^n \|\Delta \mathbf{B}_i^p - \Delta \mathbf{V}_i^p\|^2$ 
10:  Optimization:
       $(P_1, \mathbf{H}_p, P_2, \mathbf{H}_p) = \arg \min \sum_{i=1}^n \|\Delta \mathbf{B}_i^p - \Delta \mathbf{V}_i^p\|^2$ 
11:  Update for next iteration:
       $P_1^{\text{init}} = P_1; \mathbf{H}_p^{\text{init}} = \mathbf{H}_p; P_2^{\text{init}} = P_2; \mathbf{H}_p^{\text{init}} = \mathbf{H}_p;$ 
12: until Tracking End
13: return  $\mathbf{P}_1, \mathbf{H}_p, \mathbf{P}_2, \mathbf{H}_p$ 

```

According to (1), the MCE with a given angle (θ) and distance (R) in relative to a sensor has a relationship

$$\mathbf{H} \cdot \mathbf{P} = R \cdot \cos\theta \quad (19)$$

where $\|\mathbf{H}\| = 1$ and θ is the angle between \mathbf{H} and \mathbf{P} . By substituting (18) into (1), the equation can be rewritten as

$$B = \frac{B_t}{R^3} (3\cos\theta \check{\mathbf{P}} - \mathbf{H}) \quad (20)$$

where $B_t = ((\mu_r \mu_0 M_T)/4\pi)$ is a constant for a given magnet and $\check{\mathbf{P}} = (\mathbf{P}/\|\mathbf{P}\|)$ is related to the distance between the sensor and target magnet on the MCE. Thus, (1) can be expressed as

$$\|\mathbf{B}\| = \sqrt{B_x^2 + B_y^2 + B_z^2} = \lambda \frac{B_t}{R^3} \quad (21)$$

where $\lambda = (3\cos^2\theta + 1)^{1/2} \in [1, 2]$. Substituting (20) into (17), the SQR can be rewritten as

$$\text{SQR} = \frac{\left| \lambda_{p2} \frac{B_t}{R_{p2}^3} - \lambda_{p1} \frac{B_t}{R_{p1}^3} \right|}{|\mathcal{N}|}. \quad (22)$$

From (22), it can be seen that SQR is related to the orientation (θ) of the target MCE and the target-sensor distance (R_{p1} and R_{p2}).

We quantified the inherent noise level of the system by comparing the output value with a theoretical value of the sensor array over more than 100 times measurement. This will also be used in the next section of the simulation to evaluate the impact of the S-D value on the localization result under this inherent noise.

During inherent noise characteristic, the error rate is defined to evaluate the intrinsic noise of the sensor, which can be expressed as follows:

$$\text{err_rate} = \left| \frac{B_{\text{measure}} - B_{\text{theory}}}{B_{\text{theory}}} \right| \times 100\% \quad (23)$$

where B_{measure} and B_{theory} indicate the measured value and the theoretical value in a fixed position, respectively. During the

system calibration, the initial orientation matrix for each sensor, sensitivity coefficient, and the magnetic moment constant M_t are obtained before the experiments and used as preset parameters for the simulation.

The measured results are shown in Fig. 3. The blue dotted line in the figure is the measured value, while the red straight line is the average error rate. The average error rate for X -, Y -, and Z -axes are 2.38%, 3.63%, and 3.61%, respectively.

To investigate how the SQR affects the localization accuracy and the validity of the results, a simulation analysis of SQR is conducted and explained in Section III.

III. SIMULATION

According to (22), SQR is affected by the target orientation and the distance of the target moving between positions P_1 and P_2 , namely, the S-D. Thus, we have

$$\frac{1}{SQR} = \left| \frac{\mu_{p1} R_{p2}^3 - \mu_{p2} R_{p1}^3}{R_{p2}^3 - R_{p1}^3} \right| \quad (24)$$

where μ_{p1} and μ_{p2} represent the inherent noise intensity at positions P_1 and P_2 , respectively. With $\mu = \mu_{p1} - \mu_{p2}$, (24) can be rewritten as

$$\frac{1}{SQR} = |\mu_{p1}| + \left| \frac{\mu R_{p1}^3}{R_{p2}^3 - R_{p1}^3} \right|. \quad (25)$$

It can be seen from (25) that, with any specific inherent noise, the increment of the distance between the targets at the moment increases the value of SQR (i.e., $|R_{p2}^3 - R_{p1}^3| \uparrow \Rightarrow SQR \uparrow$).

In the simulation, MATLAB (MathWorks Inc., United States) is used. Since the movement of the capsule in the patient body is driven by the peristalsis of the gastrointestinal tract, this squeezing and wavering motion prevents the orientation from changing dramatically [28]. Therefore, the orientation of the magnetic target is assumed to not change rapidly, and the change in the orientation between adjacent sampling moment is limited to the range of $[-30^\circ, 30^\circ]$ in simulation.

Based on the result of measured inherent noise of sensor array in Fig. 3 (x -axis: 2.38%, y -axis: 3.63%, and z -axis: 3.61%), without loss of generality, the inherent noise is set to a random value between -10% and $+10\%$ of the theoretical value. The impact of S-D on the positioning accuracy was evaluated by quantifying the SQR in the simulation.

The simulation is conducted by changing the S-D to be 5, 10, 20, and 40 mm, respectively. In the simulation, the MCE is set in a plane at a fixed distance from the plane of the multiple-sensor array. The range of the MCE movement is limited in an area of $120 \text{ mm} \times 120 \text{ mm}$. The Euclidean distance $\text{Err}_{\text{pos}_i} = \|P'_i - P_i\|$ and included angle $\theta_i = \text{acos}(\mathbf{H}'_i \cdot \mathbf{H}_i)$ are calculated to quantify the positioning accuracy and angular accuracy (P'_i , \mathbf{H}'_i : preset position and orientation; P_i , \mathbf{H}_i : simulated position and orientation).

The simulation results are summarized in Figs. 4 and 5.

It can be found from Fig. 4 that the localization results of (b), (c), and (d) are better than those of (a). The reason is that, when the S-D is less than 5 mm, the SQR becomes

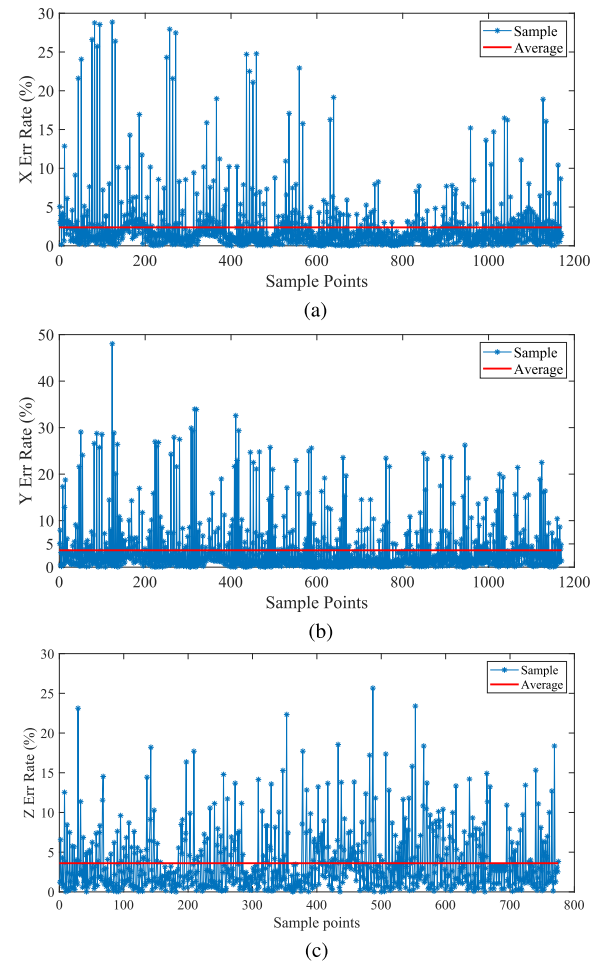


Fig. 3. Measurement of the error rate for X -, Y -, and Z -axes by an array of eight magnetoresistive sensors. (a) X -axis error rate. (b) Y -axis error rate. (c) Z -axis error rate.

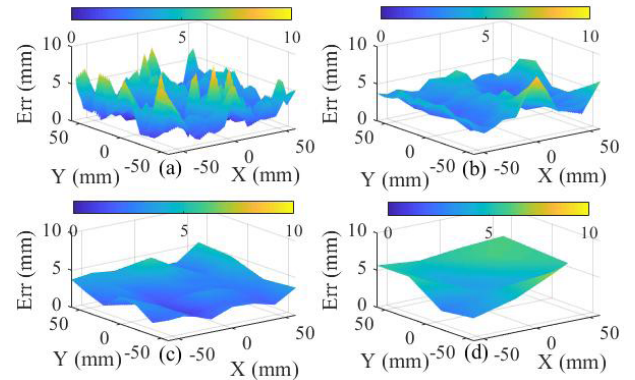


Fig. 4. Simulation result of the position error. (a) $S-D = 5 \text{ mm}$. (b) $S-D = 10 \text{ mm}$. (c) $S-D = 20 \text{ mm}$. (d) $S-D = 40 \text{ mm}$.

extremely poor, damaging the system's ability to suppress the noise. Moreover, simulation analysis for the sampling distance less than 5 mm shows that the positioning results are volatile, which caused significant errors or even complete failures in positioning.

IV. EXPERIMENTS

To confirm the simulation results, the proposed method was also tested at different S-Ds in physical experiments. In addition, the method was also investigated under the interference

TABLE I

COMPARISON OF AVERAGE POSITION AND ORIENTATION ACCURACY BETWEEN THE PROPOSED APPROACH AND THE TRADITIONAL METHOD

| Method | Position error (mm) | | | | Orientation error (°) |
|--------------|---------------------|---------|---------|-------------|--------------------------|
| | X axis | Y axis | Z axis | Eu-distance | |
| Conventional | 0.8±0.5 | 0.7±0.6 | 0.4±0.4 | 1.3±2.0 | 1.4±0.6 |
| S-D = 10 mm | 1.0±0.8 | 2.1±1.7 | 1.9±1.4 | 3.3±1.9 | 4.4±3.4 |
| S-D = 20 mm | 1.1±1.1 | 2.0±1.5 | 1.6±1.2 | 3.1±1.7 | 4.2±2.9 |
| S-D = 40 mm | 1.5±1.6 | 2.1±1.8 | 1.1±0.9 | 3.1±2.3 | 4.2±3.5 |

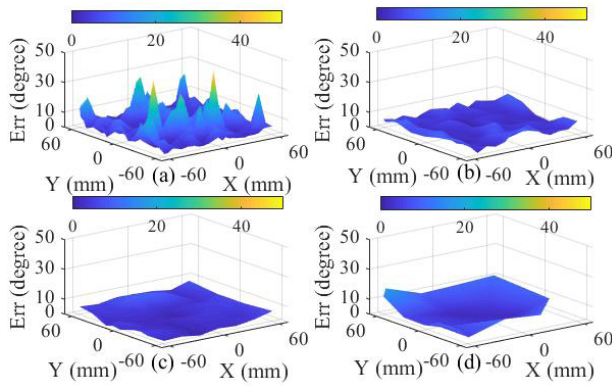


Fig. 5. Simulation result of the orientation error. (a) S-D = 5 mm. (b) S-D = 10 mm. (c) S-D = 20 mm. (d) S-D = 40 mm.

of different types of BGN to evaluate the advantages of the proposed method in terms of noise cancellation.

A. Two-Point Simultaneous Localization

In the experiments, we tracked 169 sampling points in a plane that is 88 mm away from the sensor array plane. These sampling points are evenly distributed in an area of 120 mm × 120 mm with an interval of 10 mm. A magnet with a volume of $\phi 10 \text{ mm} \times 10 \text{ mm}$ made by NdFeB is placed on these sampling points sequentially. These scales were intentionally selected to meet the size limit for the swallowable capsule endoscope (i.e., diameter < 12 mm and length < 30 mm). Based on our previous study [27], the sensor array is equally distributed in a circular shape with a diameter of 20 mm to achieve an optimal tracking performance. In experiments, the magnetic strength of these sampling points was recorded as in the conventional single-point tracking algorithm. The proposed tracking algorithm was applied to different S-Ds to optimize the position and orientation of the target.

The localization results collected from the experiments are shown in Fig. 6, where red dots are the ground truth for assessment of the localization accuracy, and blue dots are the measured values. It can be seen from Fig. 6 that, when the S-D is 10, 20, and 40 mm, most sampling points are located close to the real positions. We also tested the proposed localization algorithm when the S-D is shorter than 5 mm and found that the localization accuracy of most points is unsatisfactory due to the lower SQR . The experimental results are consistent with the simulation conclusions. Besides SQR , there are also slight errors in the magnetic positioning system, which may cause the estimated result to be different from

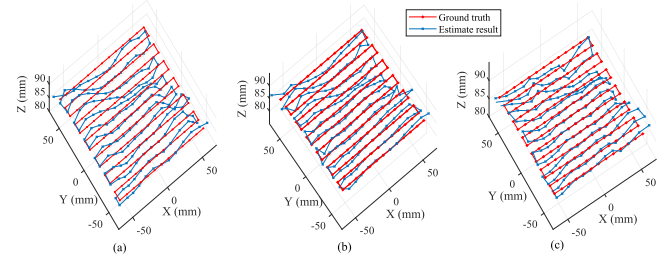


Fig. 6. Experimental results of the trajectory tracking under different S-D. (a) S-D = 10 mm. (b) S-D = 20 mm. (c) S-D = 40 mm.

the ground truth. The conventional method of single-point localization was also tested to evaluate the tracking accuracy of this magnetic tracking system. The localization results of the proposed approach compared with the conventional method are shown in Table I.

As shown in Table I, both the position accuracy and orientation accuracy are relatively stable when the S-D varies from 10 to 40 mm. Considering that the gastrointestinal examination does not require super high accuracy, the localization results from the proposed method (<3.3 mm for average positioning error and <4.4° for average orientation error) are acceptable for most medical applications. Although the positioning error of the proposed method is slightly higher than that of the traditional method in a static environment, the proposed two-point simultaneous localization approach is robust to different noisy environments.

Soft iron materials are a disturbance to the magnetic field for the localization of the magnetic target. To further examine the influence of the soft iron, the simultaneous localization experiment was conducted by placing a coin that is made of Nickel clad steel around the permanent magnet (e.g., at the center of the sensor array.) The tracking result is shown in Fig. 7. The average position error is $4.06 \pm 0.29 \text{ mm}$, and the average orientation error is $5.63^\circ \pm 4.24^\circ$. The results indicate that the system can still track the target with an acceptable performance with the soft iron materials existing in the workspace. In experiments, we also observed that, when the coin was far away from the sensor array (e.g., beyond twice the distance of the magnet and the sensor array), there were no detected changes, and the disturbance of the soft iron could be ignored.

B. Localization in Changed Noise Field

In Section IV-A, we proved the possibility of two-point simultaneous localization under the purely and distorted BGN.

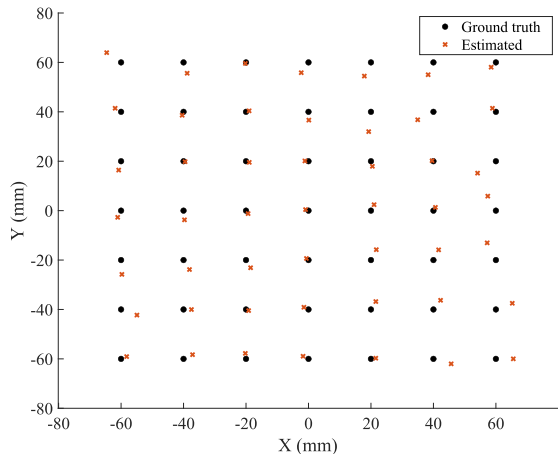


Fig. 7. Experimental results under distorted field by soft iron.

Here, in this section, we will evaluate the performance of the simultaneous localization algorithm in BGN removal and higher tracking results compared with conventional methods. In conventional static tracking systems, the surrounding environment magnetic field is carefully calibrated and removed before tracking the target. In addition, the sensor array should be stationary during the tracking process. If the sensor array moves, a tedious recalibration is needed. For medical applications of a wearable system, however, it is impractical or impossible to constrain the patient's movement during the entire gastrointestinal examination. To improve the performance of the tracking system for a real clinical scenario, the proposed algorithm is developed to tolerate a large varying BGN, allowing the patient to have a comfortable user experience with movement during the examination.

1) Geomagnetic Noise: Geomagnetism is a magnetic field that exists ubiquitously and is difficult to shield. In particular, the density of the geomagnetic field varies in different positions and different directions. How to accurately remove the geomagnetic field from the raw measurement is particularly important for improving the performance of the mobile localization system.

In experiments, we tested the proposed method with the sensor array positioned at a fixed location but with varying directions (see Fig. 8). This testing is to simulate the situation when the wearable device has an orientation shift when the device is worn. In experiments, the capsule magnet is manually moved in a mold along a regular trajectory. The moving speed is controlled in a range of 4–8 mm/s to stimulate the moving of the capsule robot. During the movement of the MCE, we randomly select a period to rotate the sensor array to simulate the varying geomagnetic noise in real applications. While the sensor array is rotating, the MCE continues to move at the prementioned range of speed.

Fig. 9 shows the tracking trajectories before and after geomagnetic noise changes, while Fig. 10 illustrates the tracking error of the experimental process. The results from both figures show that both conventional and proposed algorithms are able to achieve consistently high accuracy with the positioning error for most sampling points before BGN changed. During the rotation of the sensor array, the proposed algorithm may

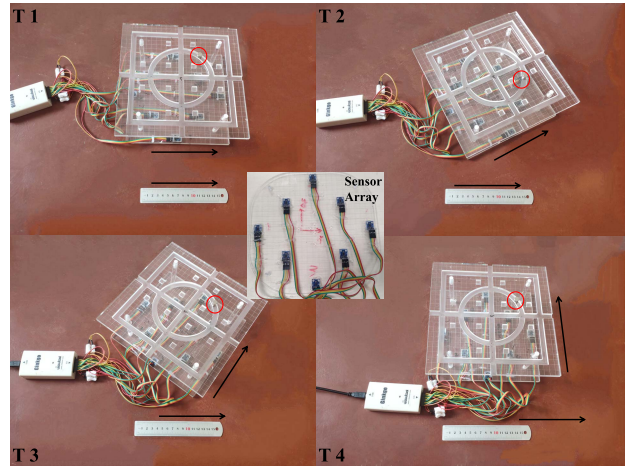


Fig. 8. Experiments of moving the sensor array to simulate the interference of changing geomagnetic noise. From T1 to T4, the sensor array is rotated ninety degrees counterclockwise, while the target magnet (shown in red circles) is moving at a speed of 4–8 mm/s. The middle inset is the layout of the sensor array.

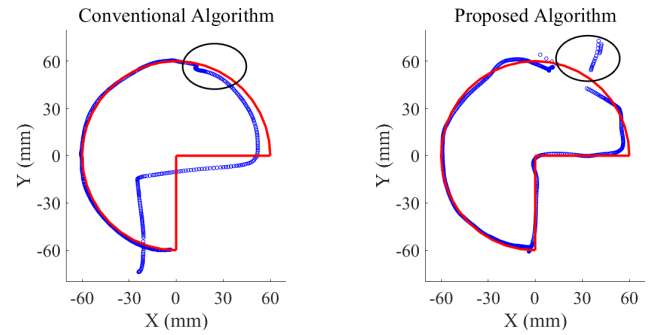


Fig. 9. Localization results under the influence of the noise caused by the changing geomagnetic field. The red curves in both figures are the true movement trajectory of the MCE. The black ellipses indicate the moment when the sensor array was rotated. When the background magnetic field changes, the error of the conventional positioning method (i.e., blue points in left figure) keeps escalating, whereas the proposed method (i.e., blue points in the right figure) can quickly reduce the error to the previous level where no noise was introduced.

lead to a short period of disturbance in localization (e.g., the black circle in Fig. 9). In contrast, the conventional algorithm continues to drift, and the tracking errors keep escalating (see Fig. 10).

One possible solution to reduce this sharp drift (see Fig. 9) in the endoscopic examination is to combine it with the information extracted from the images. When the image series do not reveal abrupt changes, the system will reject the false magnetic measurement. In other cases when the disturbance (e.g., electromagnet noise) can be regarded as white noise, additional optimization algorithms, such as Kalman filters, can be used to mitigate the noise and estimate the true state of the locations.

2) Permanent Magnet Noise: Other environmental noise in the magnetic field, such as permanent magnets or electromagnetic equipment, can also affect the accuracy of the magnetic positioning system. To simulate the situation where a patient enters a noise field with external interference, we placed a permanent magnet (material: NdFeB, diameter: $\phi 10$ mm, and

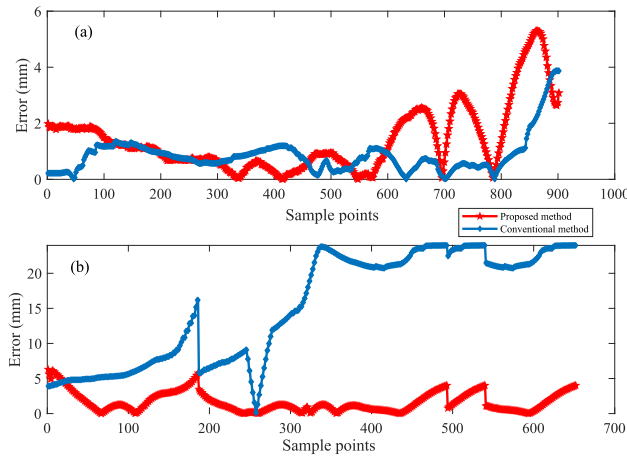


Fig. 10. Tracking errors of the proposed method (i.e., red line) and traditional method (i.e., blue line) with BGN caused by the geomagnetic noise. The tracking error is defined as the shortest distance between the experimentally measured position and the actual trajectory. (a) BGN level kept. (b) After BGN varied.

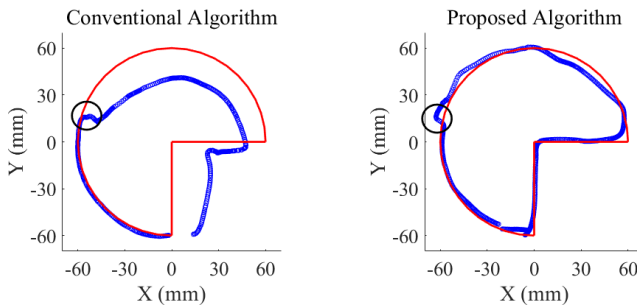


Fig. 11. Localization result under the influence of the noise caused by the permanent magnet. The tracking results of the proposed algorithm (i.e., blue points in the right figure) are more accurate than that of the conventional single-point localization algorithm (i.e., blue points in the left figure). The red curves in both figures are the true movement trajectory of the magnet target. The black ellipses indicate the moment when the permanent magnet was added to the tracking area.

length: 3 mm) in the tracking area and monitored the tracking performance.

A comparison of tracking trajectories (see Fig. 11) and localization errors (see Fig. 12) between the conventional single-point method and the proposed method revealed that the tracking accuracy of the conventional method is significantly influenced by the noise from the permanent magnet. In contrast, the proposed method is only affected during the short time when the permanent magnet is placed. When the permanent magnet is fixed in the tracking area, the positioning accuracy is reduced to the level when the permanent magnet is not placed (see Fig. 12).

V. DISCUSSION

The multipoint simultaneous localization method has the advantage of minimizing the influence of BGN on tracking accuracy. Therefore, it has robustness in a dynamically changing environment. The experimental results suggest that the proposed method achieves sufficient accuracy when following a given trajectory. We also tested the computational efficiency of the multipoint localization method on a laptop (Intel i5-4200U core CPU @ 1.60 GHz based on Windows 7). Although

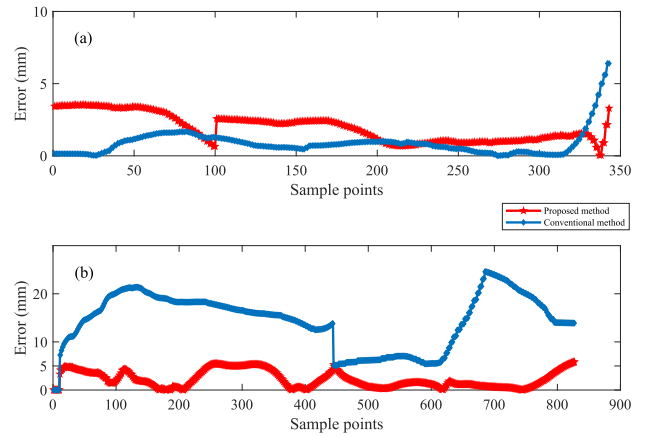


Fig. 12. Tracking errors of the proposed method (i.e., red line) and traditional method (i.e., blue line) under the interference of the permanent magnet. The proposed method remains to have a low level of tracking errors, whereas the traditional method fails to track the magnetic target. (a) BGN level kept. (b) After BGN varied.

TABLE II
TRAJECTORY-FOLLOWING ERROR COMPARISON OF THE CONVENTIONAL METHOD AND THE PROPOSED METHOD

| Noise | Method | Average Eu-distance error (mm) | |
|------------------|--------------|--------------------------------|------------|
| | | BGN kept | BGN varied |
| Geomagnetic | Conventional | 0.85±0.6 | 12.4±7.5 |
| | Proposed | 1.40±1.2 | 2.05±1.4 |
| Permanent magnet | Conventional | 0.75±0.9 | 14.71±5.7 |
| | Proposed | 1.96±0.9 | 2.22±1.7 |

the time cost for the new method is slightly higher than the conventional method, both can complete the calculation within 80 ms to achieve a fast-tracking performance. Accordingly, the proposed algorithm can be used to collect real-time data and allow patients to change their positions and orientations during a gastrointestinal examination.

The simulation results indicate that a small sampling-distance value can lead to a poor localization result because the subtraction values of two adjacent sampling points become extremely small, producing a reduced SQR value. Therefore, the selection of a suitable S-D parameter is required to avoid in practical implementation the low SQR. The requirement can be easily met by estimating the S-D value with the imaging from the onboard camera integrated into the MCE. Other solutions include the improvement of the signal-to-noise ratio by using low-noise sensors, placing more sensors, and enhancing the target's magnetic moment by changing the material and volume.

Table II summarizes the trajectory-following error from Figs. 10 and 12. The results suggest that both methods achieve a high positioning accuracy before the BGN changes. Under the interference of the changing noise, the proposed method may produce a temporary elevated error, but the system quickly restores the high-level localization accuracy once the noise stops changing. In contrast, the conventional single-point method keeps drifting when the external noise is introduced to the system.

TABLE III
COMPARISON OF STATE-OF-THE-ART MAGNETIC TRACKING METHODS WITH NOISE CANCELING

| Paper | Method | Wireless | Without additional device | Geomagnetism interference | Permanent magnet interference | DoF | Position (mm) | Orientation (°) |
|---|--|----------|---------------------------|---------------------------|-------------------------------|-----|---------------|-----------------|
| [15] | Extra IMU to measure system orientation | ✓ | ✗ | ✓ | ✗ | 5 | 3.89 | 5.5 |
| [16] | Special arranged sensor to detect geomagnetism | ✓ | ✗ | ✓ | ✗ | 5 | 5 | NA |
| [17] | Introducing the geo-noise cancellation sensors | ✓ | ✗ | ✓ | ✗ | 5 | 9.73 | 12.38 |
| [29] | Magnetic sensor module with integrated IMU | ✗ | ✗ | ✓ | ✗ | 6 | 2.6 - 5.4 | 1.89 |
| [30] | Deep Neural Network-based tongue tracking | ✓ | ✓ | ✗ | ✗ | 5 | 1.4 | NA |
| [31] | Two sensor arrays where one array for detect ambient noise | ✓ | ✗ | ✓ | ✗ | 3 | 1.01 | NA |
| [32] | Electromagnetic tracking via active coil | ✗ | ✓ | ✓ | ✓ | 5 | 0.29 | NA |
| Proposed Fusion two data sets to offset the noise | | ✓ | ✓ | ✓ | ✓ | 5 | 2.05 - 5.4 | 4.4 - 7.8 |

A comparison of the proposed method with other state-of-the-art algorithms in the previous literature is summarized in Table III. As shown in the table, the overall performance surpasses previous methods. The new method does not require additional devices, can track the untethered target, and is robust to both geomagnetic interference and permanent magnets with high accuracy.

For the positioning in the continuously changing BGN field, the sampling frequency must be higher than the rate of the BGN change. Another limitation of this study is that the phantom setup cannot simulate the complex environment inside a patient body. In the future work, the characterization of the measurement system that covers the entire gastrointestinal tract in a more realistic testing environment is necessary for the validation of the proposed method. In addition, the compatibility with other medical devices that can produce magnetic noise is also important to investigate for a further upgrade of the proposed method.

VI. CONCLUSION

In this article, we proposed a new tracking method that is robust to the interference of BGN. The proposed method removes the noise by taking the difference from two sampling points. The position and orientation of the magnet at two sampling points can be obtained at the same time by nonlinear optimization. In the simulation experiment, we analyzed the signal-to-noise ratio of the localization system at different S-Ds and found that the optimal performance was achieved at the middle range (e.g., in the range of 10–20 mm). The two-point localization method was also tested using an experimental setup with different S-Ds (i.e., 10, 20, and 40 mm).

The results suggest that the system consistently achieved low tracking errors for all the S-Ds. To simulate the interference of noise in a realistic environment, we conducted the experiments with the variations of geomagnetic noise and external noise caused by another permanent magnet. Compared with the conventional method that relies on a single-point measurement, the proposed method achieves an improved tracking accuracy and is robust in a dynamically changing background. In the future, we will integrate the optimized tracking algorithm into the wearable sensing system and test the tracking performance in clinical settings.

REFERENCES

- [1] S. Yim and M. Sitti, "Shape-programmable soft capsule robots for semi-implantable drug delivery," *IEEE Trans. Robot.*, vol. 28, no. 5, pp. 1198–1202, Oct. 2012.
- [2] S. Yim and M. Sitti, "Design and rolling locomotion of a magnetically actuated soft capsule endoscope," *IEEE Trans. Robot.*, vol. 28, no. 1, pp. 183–194, Feb. 2012.
- [3] M. C. Hoang *et al.*, "Independent electromagnetic field control for practical approach to actively locomotive wireless capsule endoscope," *IEEE Trans. Syst., Man, Cybern. Syst.*, vol. 51, no. 5, pp. 3040–3052, May 2021.
- [4] I. S. M. Khalil *et al.*, "Mechanical rubbing of blood clots using helical robots under ultrasound guidance," *IEEE Robot. Autom. Lett.*, vol. 3, no. 2, pp. 1112–1119, Apr. 2018.
- [5] K. Pahlavan *et al.*, "RF localization for wireless video capsule endoscopy," *Int. J. Wireless Inf. Netw.*, vol. 19, no. 4, pp. 326–340, Dec. 2012.
- [6] R. Chandra, A. J. Johansson, M. Gustafsson, and F. Tufvesson, "A microwave imaging-based technique to localize an in-body RF source for biomedical applications," *IEEE Trans. Biomed. Eng.*, vol. 62, no. 5, pp. 1231–1241, May 2015.
- [7] T. D. Than, G. Alici, H. Zhou, S. Harvey, and W. Li, "Enhanced localization of robotic capsule endoscopes using positron emission markers and rigid-body transformation," *IEEE Trans. Syst., Man, Cybern. Syst.*, vol. 49, no. 6, pp. 1270–1284, Jun. 2019.

- [8] V. Schlageter, P.-A. Besse, R. S. Popovic, and P. Kucera, "Tracking system with five degrees of freedom using a 2D-array of Hall sensors and a permanent magnet," *Sens. Actuators A, Phys.*, vol. 92, nos. 1–3, pp. 37–42, Aug. 2001.
- [9] C. Hu, M. Li, S. Song, W. Yang, R. Zhang, and M. Q.-H. Meng, "A cubic 3-axis magnetic sensor array for wirelessly tracking magnet position and orientation," *IEEE Sensors J.*, vol. 10, no. 5, pp. 903–913, May 2010.
- [10] K. M. Popek, T. Hermans, and J. J. Abbott, "First demonstration of simultaneous localization and propulsion of a magnetic capsule in a lumen using a single rotating magnet," in *Proc. IEEE Int. Conf. Robot. Autom. (ICRA)*, May 2017, pp. 1154–1160.
- [11] C. Di Natali, M. Beccani, N. Simaan, and P. Valdastri, "Jacobian-based iterative method for magnetic localization in robotic capsule endoscopy," *IEEE Trans. Robot.*, vol. 32, no. 2, pp. 327–338, Apr. 2016.
- [12] D. Son, S. Yim, and M. Sitti, "A 5-D localization method for a magnetically manipulated untethered robot using a 2-D array of Hall-effect sensors," *IEEE/ASME Trans. Mechatronics*, vol. 21, no. 2, pp. 708–716, Apr. 2016.
- [13] N. Mahmood and S. M. Aziz, "A real-time tracking system for in vivo endofunctional capsule using magnetic sensors," in *Proc. Annu. Int. Conf. IEEE Eng. Med. Biol. Soc.*, vol. 2012, Aug./Sep. 2012, pp. 598–601.
- [14] G. Shao and Y.-X. Guo, "An optimal design for passive magnetic localization system based on SNR evaluation," *IEEE Trans. Instrum. Meas.*, vol. 69, no. 7, pp. 4324–4333, Jul. 2020.
- [15] H. Dai, C. Hu, S. Su, M. Lin, and S. Song, "Geomagnetic compensation for the rotating of magnetometer array during magnetic tracking," *IEEE Trans. Instrum. Meas.*, vol. 68, no. 9, pp. 3379–3386, Sep. 2019.
- [16] X. Wu, W. Hou, C. Peng, X. Zheng, X. Fang, and J. He, "Wearable magnetic locating and tracking system for MEMS medical capsule," *Sens. Actuators A, Phys.*, vol. 141, no. 2, pp. 432–439, Feb. 2008.
- [17] G. Shao, Y. Tang, L. Tang, Q. Dai, and Y.-X. Guo, "A novel passive magnetic localization wearable system for wireless capsule endoscopy," *IEEE Sensors J.*, vol. 19, no. 9, pp. 3462–3472, May 2019.
- [18] J. Kramer and A. Kandel, "Robust small robot localization from highly uncertain sensors," *IEEE Trans. Syst., Man, Cybern., C, Appl. Rev.*, vol. 41, no. 4, pp. 509–519, Jul. 2011.
- [19] C. Hu *et al.*, "Locating intra-body capsule object by three-magnet sensing system," *IEEE Sensors J.*, vol. 16, no. 13, pp. 5167–5176, Jul. 2016.
- [20] B. Fang, F. Sun, H. Liu, C. Liu, and D. Guo, "Wearable sensors," in *Wearable Technology for Robotic Manipulation and Learning*. Singapore: Springer, 2020, doi: 10.1007/978-981-15-5124-6_2.
- [21] J. Lu, Z. Yang, K. Z. Okkelberg, and M. Ghovalloo, "Joint magnetic calibration and localization based on expectation maximization for tongue tracking," *IEEE Trans. Biomed. Eng.*, vol. 65, no. 1, pp. 52–63, Jan. 2018.
- [22] H.-T. Chang and J.-Y. Chang, "Sensor glove based on novel inertial sensor fusion control algorithm for 3-D real-time hand gestures measurements," *IEEE Trans. Ind. Electron.*, vol. 67, no. 1, pp. 658–666, Jan. 2020.
- [23] J.-H. Zhang, P. Li, C.-C. Jin, W.-A. Zhang, and S. Liu, "A novel adaptive Kalman filtering approach to human motion tracking with magnetic-inertial sensors," *IEEE Trans. Ind. Electron.*, vol. 67, no. 10, pp. 8659–8669, Oct. 2020.
- [24] K. Chen, S. N. Patel, and S. J. Keller, "Finexus: Tracking precise motions of multiple fingertips using magnetic sensing," in *Proc. Conf. Hum. Factors Comput. Syst. (CHI)*, 2016, pp. 1504–1514.
- [25] W. Lv, Y. Kang, and J. Qin, "Indoor localization for skid-steering mobile robot by fusing encoder, gyroscope, and magnetometer," *IEEE Trans. Syst., Man, Cybern. Syst.*, vol. 49, no. 6, pp. 1241–1253, Jun. 2019.
- [26] M. Wang, Q. Shi, S. Song, and M. Q.-H. Meng, "A novel magnetic tracking approach for intrabody objects," *IEEE Sensors J.*, vol. 20, no. 9, pp. 4976–4984, May 2020.
- [27] S. Song, X. Qiu, J. Wang, and M. Q.-H. Meng, "Design and optimization strategy of sensor array layout for magnetic localization system," *IEEE Sensors J.*, vol. 17, no. 6, pp. 1849–1857, Mar. 2017.
- [28] J. Laplace, "Gastro-intestinal transit in monogastric animals. 2. Motor events and digesta movements," *Annales de Zootechnie*, vol. 24, no. 3, pp. 489–551, 1975.
- [29] D. A. F. Guzman, P. M. Ros, D. Demarchi, and M. Crepaldi, "A low-complexity 6DOF magnetic tracking system based on pre-computed data sets for wearable applications," *IEEE Trans. Circuits Syst. I, Reg. Papers*, vol. 67, no. 12, pp. 5065–5078, Dec. 2020.
- [30] N. Sebkhi *et al.*, "A deep neural network-based permanent magnet localization for tongue tracking," *IEEE Sensors J.*, vol. 19, no. 20, pp. 9324–9331, Oct. 2019.
- [31] A. Adel, M. Mansour, M. M. Micheal, A. Abdelmawla, I. S. M. Khalil, and S. Misra, "Magnetic localization for an electromagnetic-based haptic interface," *IEEE Magn. Lett.*, vol. 10, 2019, Art. no. 2102705.
- [32] G. Andria, F. Attivissimo, A. Di Nisio, A. M. L. Lanzolla, P. Larizza, and S. Selicato, "Development and performance evaluation of an electromagnetic tracking system for surgery navigation," *Measurement*, vol. 148, Dec. 2019, Art. no. 106916. [Online]. Available: <https://www.sciencedirect.com/science/article/pii/S0263224119307730>



Min Wang received the B.S. degree from the Hefei University of Technology (HFUT), Hefei, China, in 2017, and the M.S. degree from the Harbin Institute of Technology (Shenzhen) (HITSZ), Shenzhen, China, in 2020. He is currently pursuing the Ph.D. degree with the City University of Hong Kong, Hong Kong, SAR, China.

His main research interests include the actuation and tracking methodology for soft and microrobots.



Shuang Song received the B.S. degree in computer science and technology from North China Electric Power University, Baoding, China, in 2007, the M.S. degree in computer architecture from the Chinese Academy of Sciences, Beijing, in 2010, and the Ph.D. degree in computer application technology from the University of Chinese Academy of Sciences, Beijing, in 2013.

He is currently an Associate Professor with the Harbin Institute of Technology (Shenzhen), Shenzhen, China. His main research interests include magnetic tracking and actuation for bioengineering applications, such as surgical robots and micromanipulation.



Jun Liu (Member, IEEE) received the Ph.D. degree from the University of Toronto, Toronto, ON, Canada, in 2016.

He was a Post-Doctoral Fellow with the Dalio Institute of Cardiovascular Imaging, Cornell University, Ithaca, NY, USA, from 2017 to 2019. He is currently an Assistant Professor with the City University of Hong Kong, Hong Kong. His research interests include micro-nano-robotics, and medical image analysis and interaction.

Dr. Liu has won multiple awards, including the Best Student Paper Award and the Best Medical Robotics Paper Finalist Award from the IEEE International Conference on Robotics and Automation in 2014 and the IEEE TRANSACTIONS ON AUTOMATION SCIENCE AND ENGINEERING Best New Application Paper Award in 2018.



Max Q.-H. Meng (Fellow, IEEE) received the Ph.D. degree in electrical and computer engineering from the University of Victoria, Victoria, BC, Canada, in 1992.

He is currently a Chair Professor and the Head of the Department of Electronic and Electrical Engineering, Southern University of Science and Technology, Shenzhen, China, on leave from the Department of Electronic Engineering, The Chinese University of Hong Kong, Hong Kong. He has published more than 750 journal articles, conference papers, and book chapters and led more than 60 funded research projects to completion as a principal investigator. His research interests include robotics, perception, and intelligence.

Dr. Meng is a fellow of the Hong Kong Institution of Engineers and an Academician of the Canadian Academy of Engineering. He was a recipient of the IEEE Millennium Medal. He has served as an Associate VP for Conferences of the IEEE Robotics and Automation Society from 2004 to 2007, the Co-Chair of the Fellow Evaluation Committee, and an elected member of the AdCom of IEEE Robotics and Automation Society.